The Artificial Inducement of a Local Space Warp Bubble Using a VEM Drive

David Pares, Kyle Finley and Matthew Judah

Tables of contents

Abstract

This paper describes a new solid-state, zero propellant, radio-frequency (RF) resonant, variable near field reactants and Variable Electro Magnetic Drive (VEM) Drive. The VEM Drive creates a pulling action within the framework of general relativity. The authors demonstrate how it is possible to create a pulling force in front of the VEM Drive. The data collected shows an artificial inducement to compress local space. This tendency creates a local space warp bubble. Laboratory investigations and preliminary findings confirm the hypothesis that the resultant, VEM Drive pulling force is accomplished using fractal tri-pole electric fields, which can adjust the near field reactants along with a throttle control and a 48 Volt, 160 Amp Hour battery pack. The pulling-to-power results, at 20 seconds of continuous power are .19 N at 100 watts to 6.25 N at 1650 watts mode at 146 MHz for VEM Drive. A further comparison will be made between other Ion and EM Drives.

Keywords: general relativity, zero propellant Drive, radio-frequency (RF) resonant, variable near field reactants, VEM Drive, EM Drive

The Artificial Inducement of a Local Space Warp Bubble Using a VEM Drive

Alcubierre (1994), Van den Broeck (1999), Obousy and Cleaver (2007) expound the possibility of faster than light travel using the theoretical concept of space warp. Mathematically hypothesizing space warp, Alcubierre (1994) receives credit for popularizing the concept of faster than light travel. While physicists commonly dismiss the idea of space warp because of high-energy requirements, this criticism does not stop researchers from exploring the practical applications including how humans can traverse the vast distances of the cosmos (Van den Broeck, 1999). Research and laboratory results suggest that local space warp is a naturally occurring phenomenon in strong thunderstorms (Pares, 2010).

Theoretical physicists have long held the belief that a local space warp bubble could only occur using sources of exotic energy (Pfenning & Ford, 1997). This paper summarizes evidence demonstrating warp bubbles using less than 2000 watts of power. The following section provides background information leading to the discovery of artificially induced sustainable space warp motor drive technology.

This paper describes a VEM Drive that artificially induces a local space warp bubble, demonstrating its existence utilizing measurements of red shift, magnetic field curvature and linear displacement of objects through solid material. Newly developed tri-pole fields combined with radiating near fields are used to distort space-time in such a way as to induce a local space warp bubble. The resonant RF V shape near field reactants cavity utilizes four tri-pole fractal arrays. The design of the VEM Drives emulates the overlap of two thunderstorm electric fields.

Using a modified interferometer, the shape of the compression field and red shift was detected when a laser and frequency monitoring equipment was directed through the energized arrays. The resulting data collected indicated the presence of a local micro space warp bubble. The measurable results yielded a compression metric of .097 nm/sec at 25 watts of power. These series of experiments demonstrated an ability to artificially induce a detectable warp bubble. Additional experiments with increased power expanded the influence of the local space warp bubble and produced exponential results. At 1650 watts of power, the VEM Drive produced 1.5 lbs. of pulling force.

(Included in this document are power vs force graphs, curvature of space around the engine as measured by magnetic flux, and a chart of measured gravity fields induced by the engine.)

2. Literature Review

Within the confines of special relativity, no object with mass can travel faster than light (Puthoff, 1996). The same rule is present in general relativity. However utilizing a concept of general relativity introduced by Alcubierre (1994), it can be shown that an object can travel locally faster than the speed of light through the expansion and contraction of local space. Alcubierre's warp is constructed graphically in Figure 1.1.

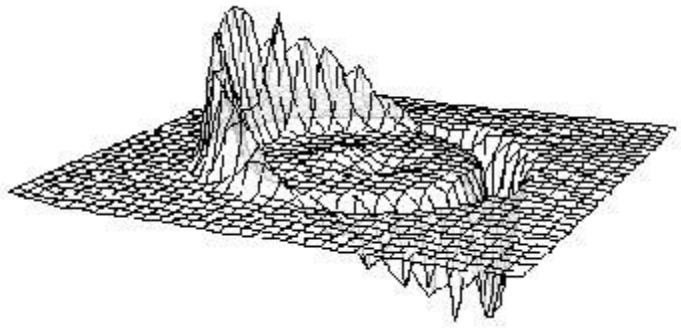

Figure 2.1. NASA depiction of the Alcubierre drive, showing the lattice of space.

The graph shows the expansion of space-time behind and compression of space-time in front of the local space warp bubble. Thus, a craft generating this distortion field is pushed forward by the expansion of space behind and pulled forward by the compression of space in front of the craft. The space-time distortion leaves the ship at rest in the center of the space-warp bubble with respect to locally flat space. There are no relativistic effects present inside of the bubble. The absence of relativistic time dilation and mass increase allows the ship to move through the expansion and contraction of space. This outcome may allow the craft to move at (or perhaps even greater than) the speed of light. Estimates over 100 times greater than speed of light have been postulated by (Puthoff, 1996) and ("Extending Einstein's theory," 2012).

Space warp has been long considered to be a purely mathematical exercise ("Extending Einstein's theory," 2012). Alcubierre's first prediction of the energy requirement necessitated an enormous amount of exotic energy to produce the space warp field (1994). Over the past two decades estimates of the amount of power needed for space warp have systematically decreased from the amount of energy in the universe, to the amount of energy in the Milky Way galaxy, to the energy equivalent of the mass of the Voyager spacecraft ("Extending Einstein's theory," 2012 and Obousy & Cleaver, 2007).

Another problem associated with the idea of space warp is the kind of device needed to create and sustain a local space warp field. Researchers have long held that this is the most problematic part of the space warp concept because an engine that could distort space-time would have to utilize exotic forms of energy such as anti-matter or the theorized "dark energy" ("Extending Einstein's theory," 2012). These two problems have long held research on space warp to a minimum.

3. Artificial Inducement of Local Space Warp

Pilot reports over the last 70 years indicate that while flying through thunderstorms, a linear displacement from 100 to 300 miles has been reported. After researching several cases the results indicated that pilots experienced a linear displacement in terrestrial space (MacGregor & Gernon, 2005, 2017) and (Pares, 2010, 2017). These cases might be a natural example of Alcubierre's Theory. These cases revealed conditions to induce a momentary non-sustainable local space warp bubble. The analysis concluded that electric fields generated by overlapping thunderstorms formed tri-pole field patterns capable of compressing the fabric of space. Forensic weather studies indicated that large thunderstorms produced the necessary electric field anomaly for an aircraft to travel using the expansion and contraction of local space. Plans evolved to fly an UAV into the same conditions surrounding these pilot accounts. It was abandoned due to operational and legal limitations (Red Tape!). However, if this, phenomena were true, then it should be able to be reproduced in a laboratory environment. The electric field patterns were reproduced in the laboratory, and the follow-on research and development produced our patent pending VEM Drive.

.

3.1 The Experiments

Initial experiments used custom built tri-pole antennas that resonated in the VHF range, just like in the middle of a thunderstorm. shown in Figure 2.

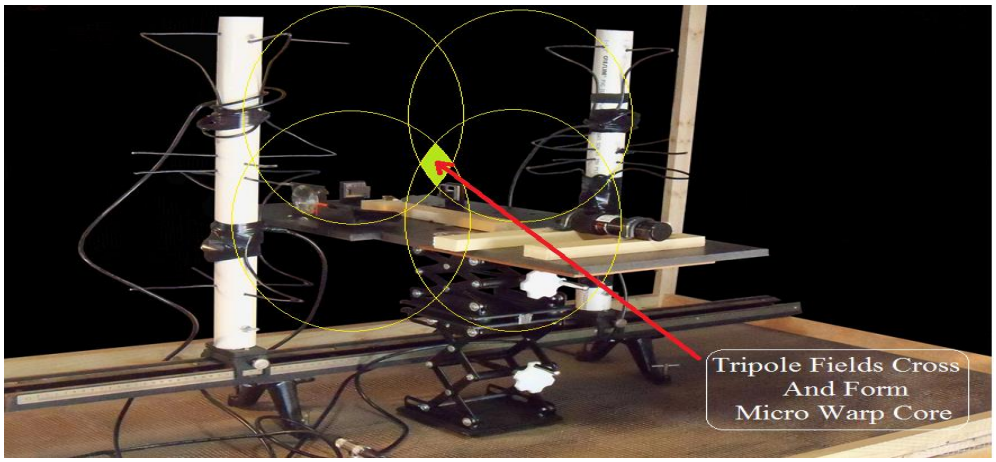

Figure 3.1.1. Interferometer Experiment Setup

The experiment replicated frequency data collected from flying into thunderstorms by our team (circa 2008-2010). A laser was used along with a modified interferometer in the experiment. The resultant data indicated a central core pattern of compression.

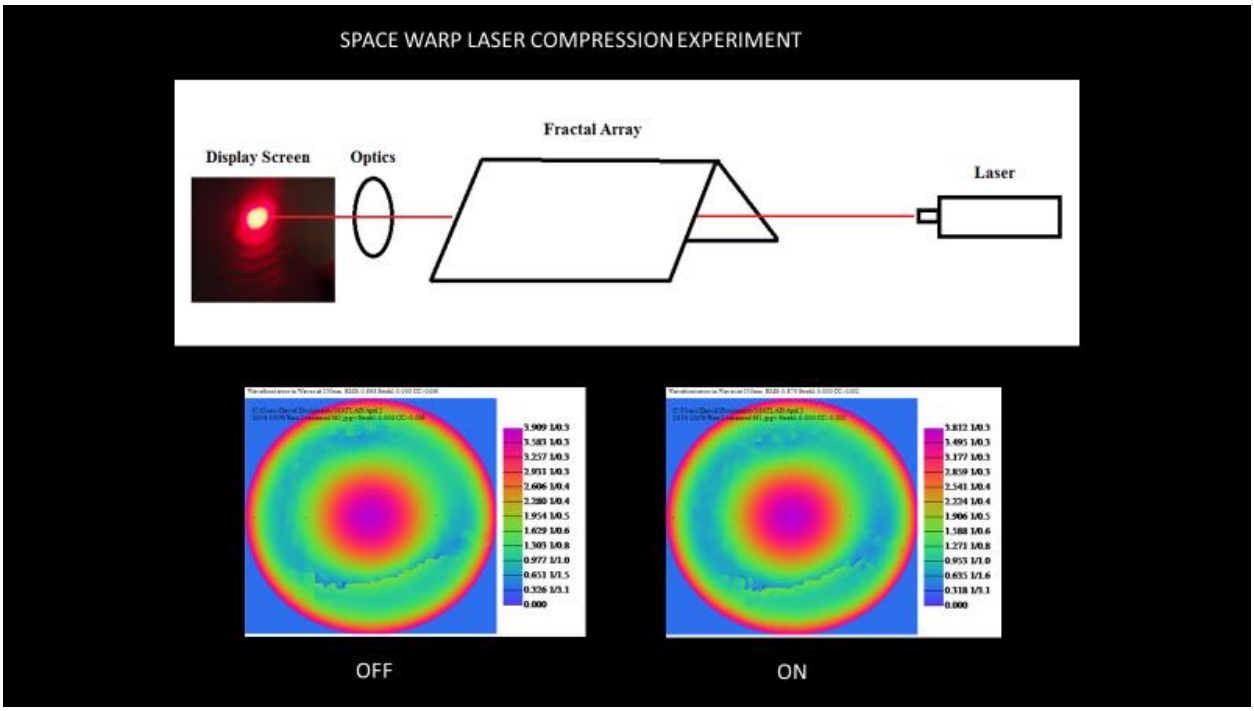

Another laser compression experiment was designed to see if the results of the first series could be validated using a different method. This next compression experiment consisted of focusing a laser through a Faraday cage that contained the fractal array and a Trifield ™ meter. The laser was aimed one inch from the base of the fractal arrays. The laser beam then passed out of the Faraday cage, through a 12 X magnifying lens and was imaged on a white projection screen. A laser fringe image was recorded using a Microsoft™ Lifecam HD ™, webcam each time the system was turned "ON" and "OFF". (See Fig. 1.4)

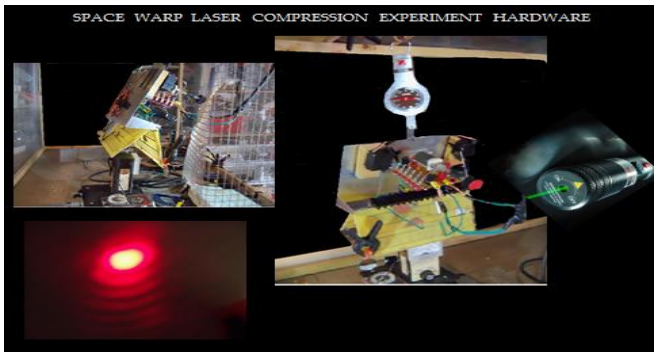

A total of 140 images were captured during the experiment which was conducted in a darkened environment. A solar panel was also used to ensure that any stray ambient light would be measured and accounted for during all the experiments. A constant value of 0.1Volts on the VOM (Volt Ohm Meter) was recorded during all the experiments.

The experiment proceeded as follows: A series of ten photographs were taken as five sets of two photographs. The set of two photographs consisted of one photograph being taken while the

array was not being engaged (OFF) and the other taken after the array had been engaged for 4 seconds (ON). Overall, seventy sets of pictures were taken. Five sets were taken at 10W and 15W of power. Eighteen sets were taken at 25W of power. Forty-four sets were taken using 100W of power.

The statistics of this experiment determined if there was a relationship between the initial (OFF) diameter and how much the fringe was compressed in total. All the data showed that the (ON) diameter was compressed when compared to the (OFF) diameter of the fringe pattern. However, the R-squared value of the (OFF) to compression relationship was only '0.43'. This demonstrated that there is a relationship between the original diameter and amount of compression in the laser beam. The compression ratio results can be explained due to the limitations of the equipment and oversaturation of the pixels in some of the webcam photographs.

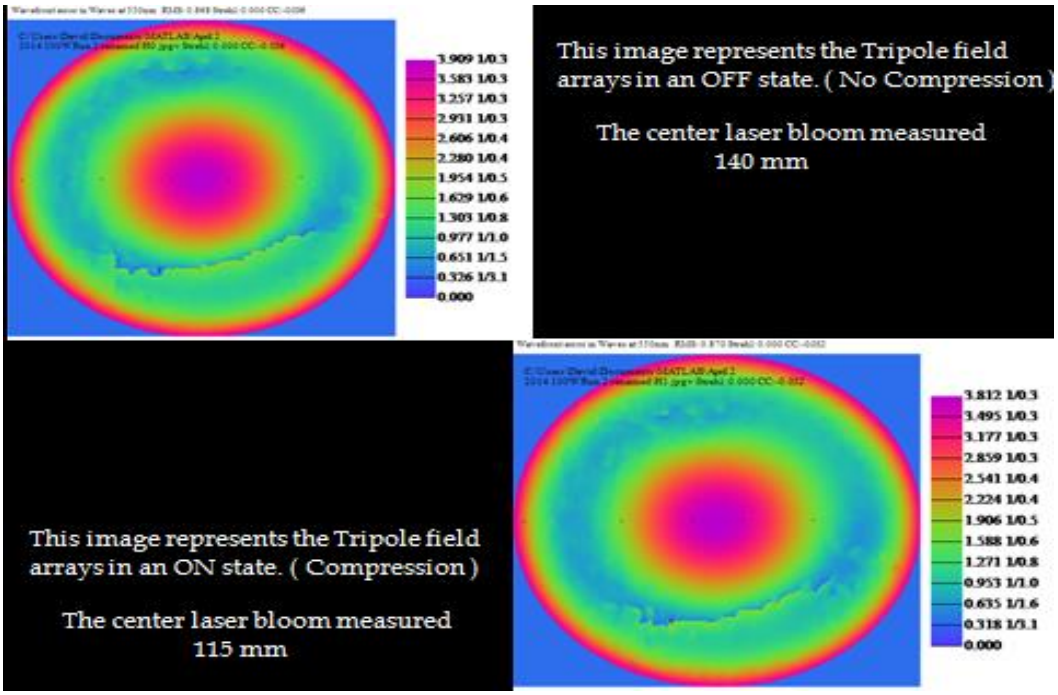

Figure 3.1.2. Interferometer Results

The chart below shows a sample of the data used to make the calculations and the resultant Sigma 4 value from 140 samples. There was correlation to the data collected. Space warp does exist.

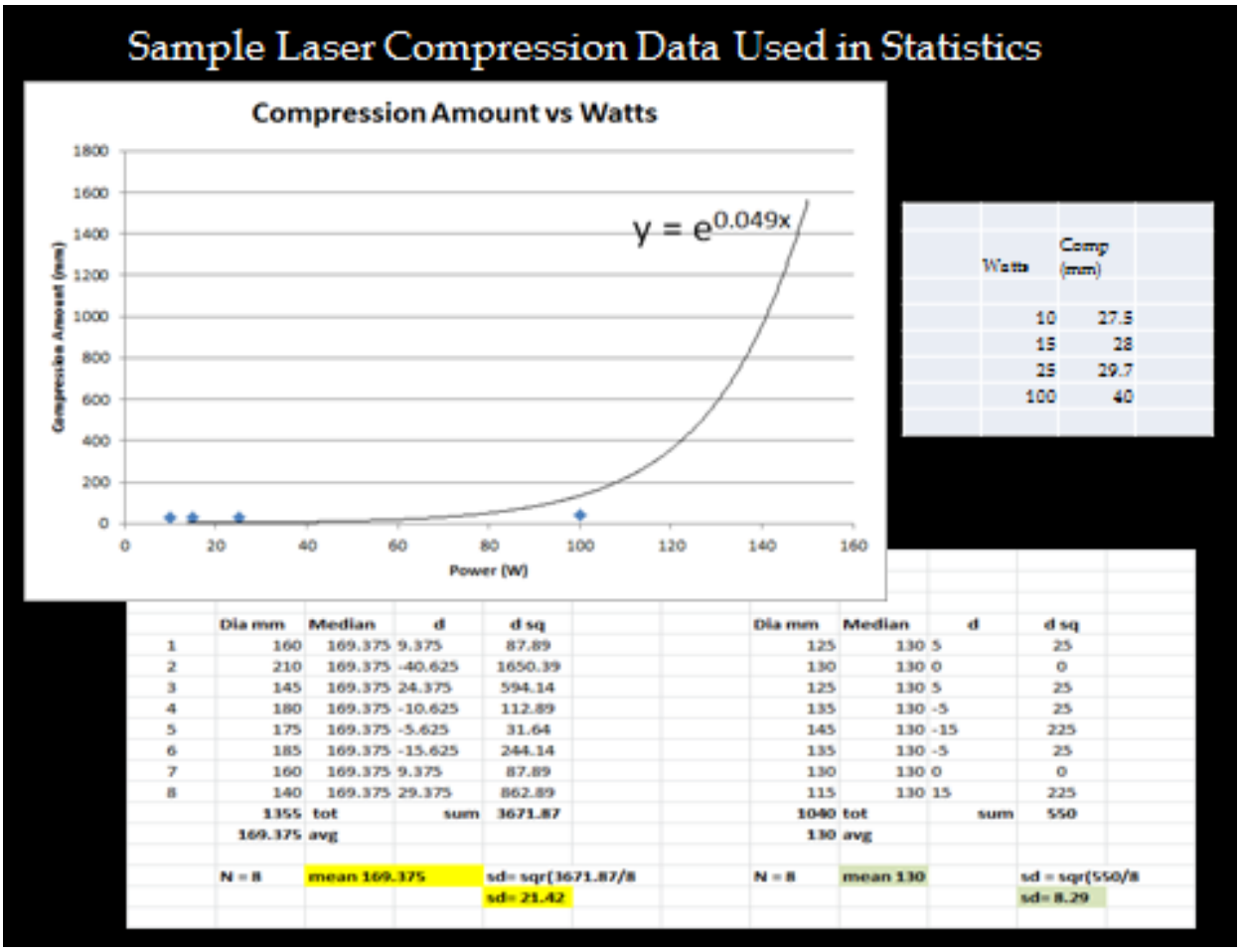

Figure 3.1.3. Data from 140 sample points taken during an experiment.

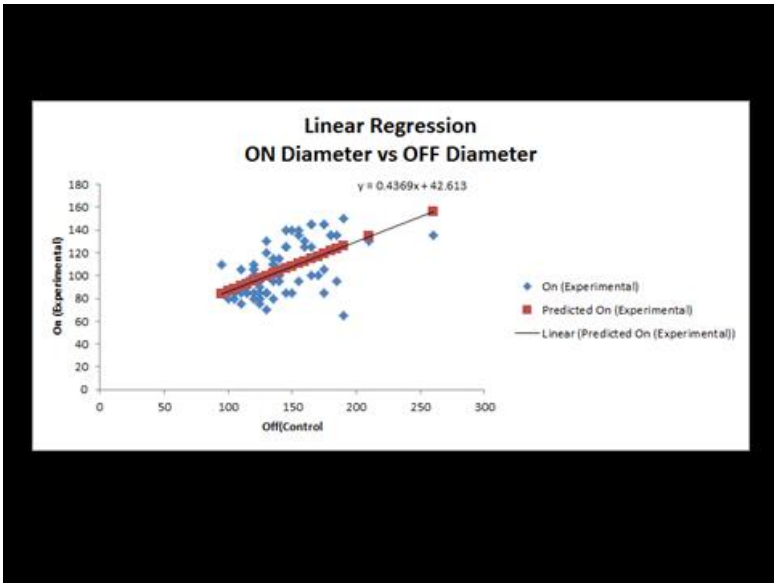

Figure 3.1.4. Regression calculation graph discussed in section.

3.2. Red Shift

The Correspondence Principle can be applied for determining the red shift in local space. Using the equation $\frac{\Delta\lambda}{\lambda} = \frac{\lambda_0 - \lambda_1}{\lambda_0}$ measurements were made of the motors output frequency and wavelength. It was unknown if any wavelength shift would be found. Confirmation of the existence of a red shift would be one key characteristic that a space warp metric did exist when the motor was activated at 5 watts of power. The measured red shift is as follows:

$$\frac{\Delta\lambda}{\lambda} = \frac{\lambda_0 - \lambda_1}{\lambda_0} = \frac{2.0483408439164275\ m - 2.0483436410537226\ m}{2.0483408439164275\ m} =$$

$$\frac{2.0483408439164275 - 2.483436410537226}{2.0483408439164275} = \textbf{-1.36556 X } \mathbf{10^{-6}}\ \textbf{m}$$

The red shift was detected into the motor. A shift from the primary 146 MHz transmit frequency.

3.3. The Near Field

There's seemingly no formal definition for the near field, it depends on the type of application of the radiative area. The most agreed upon definition submits that the near field is less than one wavelength (λ) from the source. Wavelength in meters is given by:

$$\lambda = 300/f_{MHz}$$

The distance from the array of the near field is calculated as:

$$\lambda/2\pi = 0.159\lambda \quad \text{(Standard Expression)}$$

The near field is generally said to be divided into two areas, the reactive and the radiative. In the reactive area, the E and H fields are the strongest and can be measured separately.

To compute the effective radiative near field of both tri-pole fractal arrays the following equation are as follows:

R_{nf} = SQR(2 sin $\theta^0(2D^2 / f)$) (Equation of fractal arrays radiative near fields)

R_{nf} = crossover distance between nf (near field) in meters

D = largest dimension of the transmit array (.3048 m) or (12 inches) Model 13 Engine

f= frequency ……. (VHF in MHz)

$\theta^0 = 70^0$ Angle between Fractal Arrays (The angle is dependent on fractal pad/tri-pole field spacing and the amount of power being considered.)

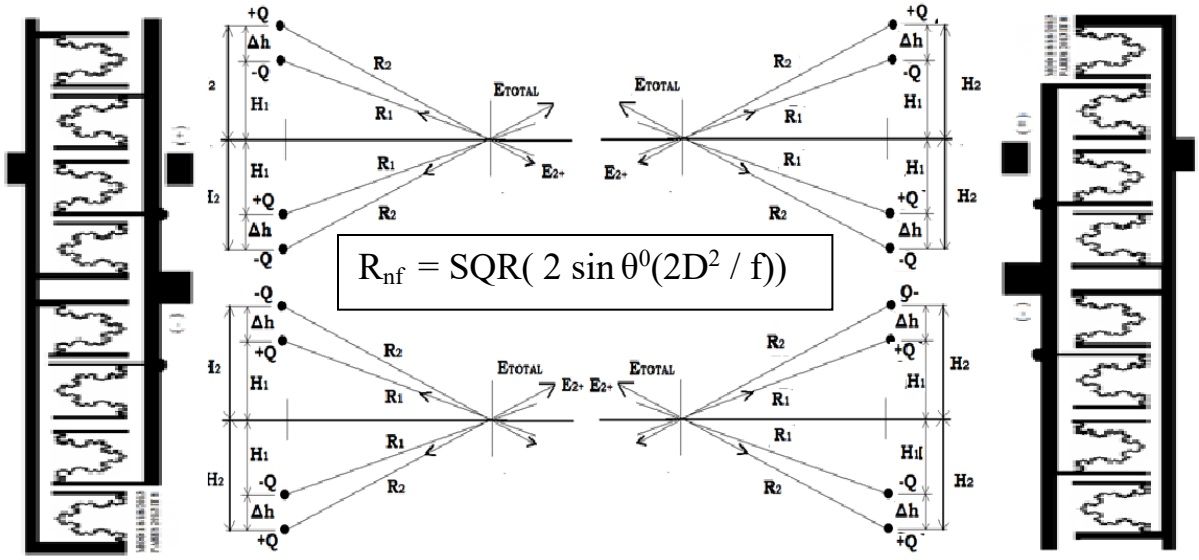

Figure 3.3.1. The diagram describes the size of the physical induced field based on angle of the arrays to each other and the reactive near field.

3.4. Modified Cavendish Experiment

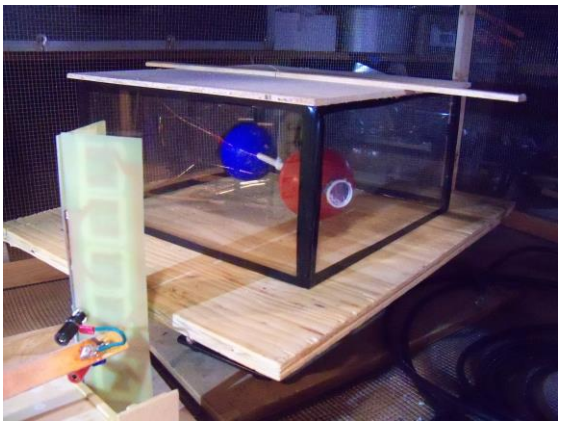

Figure 3.4.1.

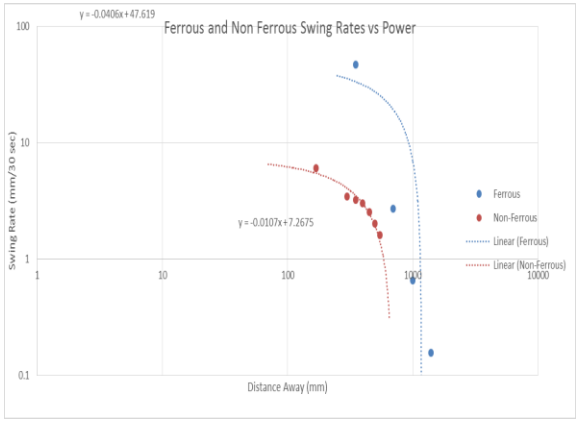

Figure 3.4.2.

An electrically insulated modified Cavendish experiment was used to demonstrate the influence of an induced local warp field to a freely suspended torsion bar with balanced 3.5-pound ferrous weights. The warp drive motor was positioned 35 cm from one of the suspended weights. A laser was used to reflect off the mirror mounted at the end of the suspended weight. The laser light was then displayed on a projection screen. In 45 seconds that the motor was active, a 7cm displacement was measured. This is a 1.5 mm per sec transit. The significance of this experiment

is very important in that the local compression field created by the VEM Drive went through a solid object and pulled the torsion bar weights toward the Drive.

The resultant, reactive near field, pulled the free weight toward the VEM Drive through an electrically insulated solid case. The Non-Ferrous material weighed 1.5 lbs. and the ferrous material weighed 3 lbs. 20 watts of power was used in the collecting the swing rates for the non-ferrous torsion bar and 100 watts was used for the ferrous. The swing rates and resulting curves show similar curves at different power levels using different materials.

As the data was analyzed it looked like a pattern started to emerge. A subsequent prediction equation was created to predict future power to distance out comes. This equation became useful in new engine design considerations.

Equation for predictions

X min/sec = K x $D^{-4.112701204}$ cm
K = 3494741.871 Constant
D = Distance from midpoint of Drive to suspended Weight
X = Speed of Swing of Weight

Table for VEM Drive Motor Fetch Influence

Distance from Motor	Speed of Swing	Swing per Minute
*35 cm	1.56 mm/sec	93.6 mm/min
*70 cm	.09 mm/sec	5.5 mm/min
*100 cm	.0216 mm/sec	1.296 mm/min
*140 cm	.0052 mm/sec	.312 mm/min

Results: * Actual measurements

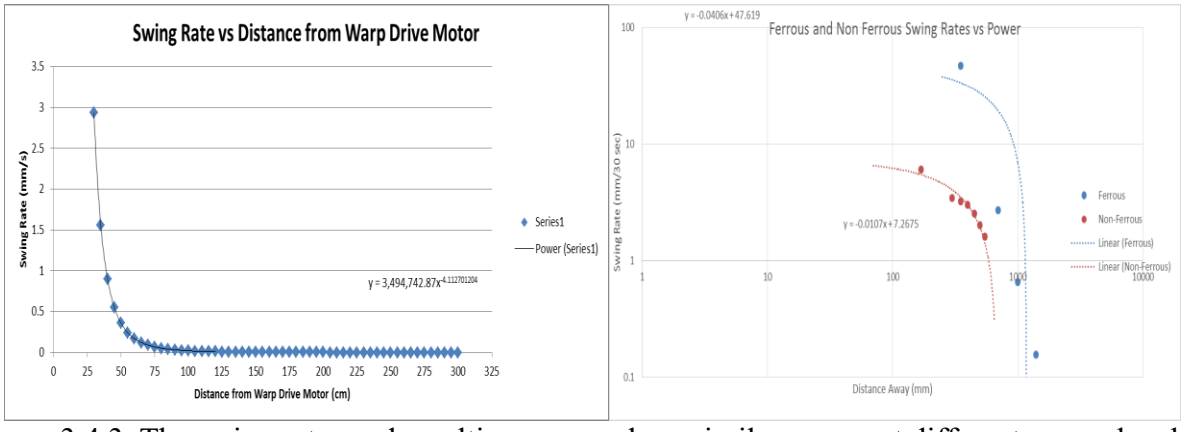

Figure 3.4.3. The swing rates and resulting curves show similar curves at different power levels using different materials.

4. Flight Control Axial Movement and Warp Bubbles

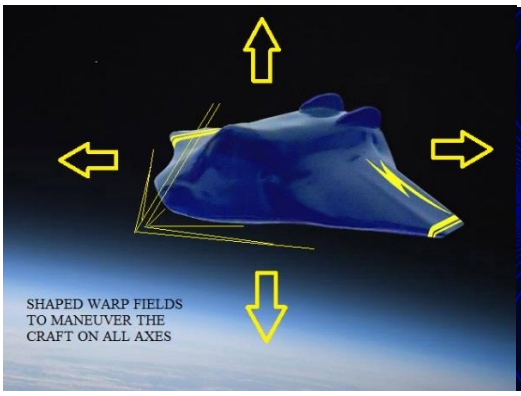

Axial Craft Maneuvering

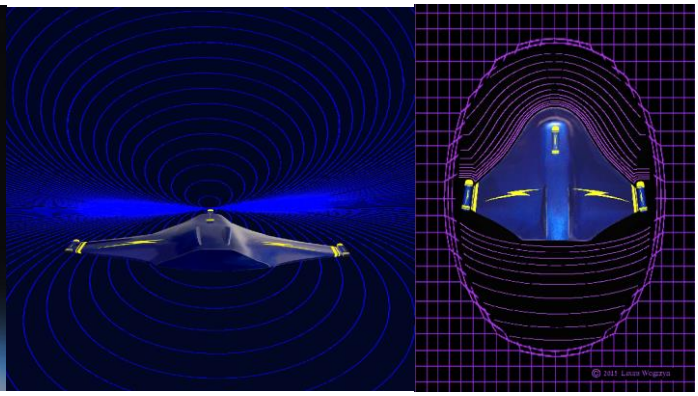

Local Spacetime Compression Fields

Tests were made with an early series of motors to see how one could maneuver in a space environment. The question was, do you need to create, one large warp bubble or can you create a series of warp bubbles to surround a space craft and maneuver by manipulating the strength of the individual fields. A test stand was setup with two motors, Motor A and Motor B in a downward position. Both were given equal power, the result no side to side motion. When Motor A was given more power, it turned to the left the strong side of the field. When Motor B was given more power respectively it turned to the right the strong side of the field. Therefore, left right up down maneuvering capability seems to be possible. Building larger warp bubbles from multiple engines sources would be a practical method to surround a spacecraft to enable full axial control while in space

VEM Drive fields can't just be activated, the field must be built over time. It takes several seconds to build the field and then run at the desired power level.

4.1. Magnetic Field Curvature

The magnetic field generated by the engine was evaluated and mapped into a 3D wire mesh image. The magnetic flux data was collected 4 inches from the bottom of the engine. A Raspberry Pie computer and Adafruit Triple-Axis Magnetometer Board - HMC5883L was used to collect the data. The engine is 2 ft. long x .5 ft. high with an adjustable opening at the bottom. For this test, the angle was set to 60 degrees which was a 5-inch opening at the bottom of the engine. It should be noted that the engine is a pulling engine, it does not thrust and is silent.

The relationship between curvature and magnetic field was derived by Minami and introduced it in 16th International Symposium on Space Technology and Science (1988), Musha,

(2011). The derived equation $R^{00} = \frac{4\pi G}{\mu_0 c^4} \cdot B^2$ was used along with the empirical magnetic flux data collected under the engine. The area covered was 2 ½ ft. by 1 ft. (55 points of 3 in. x 3 in. grid) over a 20 second period at 10 watts of power from the engine.

Equation definitions:

$R^{00} = \frac{4\pi G}{\mu_0 c^4} \cdot B^2 = 8.2\times10^{-38} \cdot B^2$

$\mu_0 = 4\pi\times10^{-7}(\text{H / m})$

$c = 3\times10^{8}(\text{m / s})$

$\varepsilon_0 = {}^{1}\!/_{(36\pi)\times10^{-9}}\ (\text{F / m})$

$G = 6.672\times10^{-11}\left({}^{N\cdot m^2}\!/_{kg^2}\right)$

B is the Magnetics field in Tesla's and

R^{00} is the major component of special curvature ($1/m^2$).

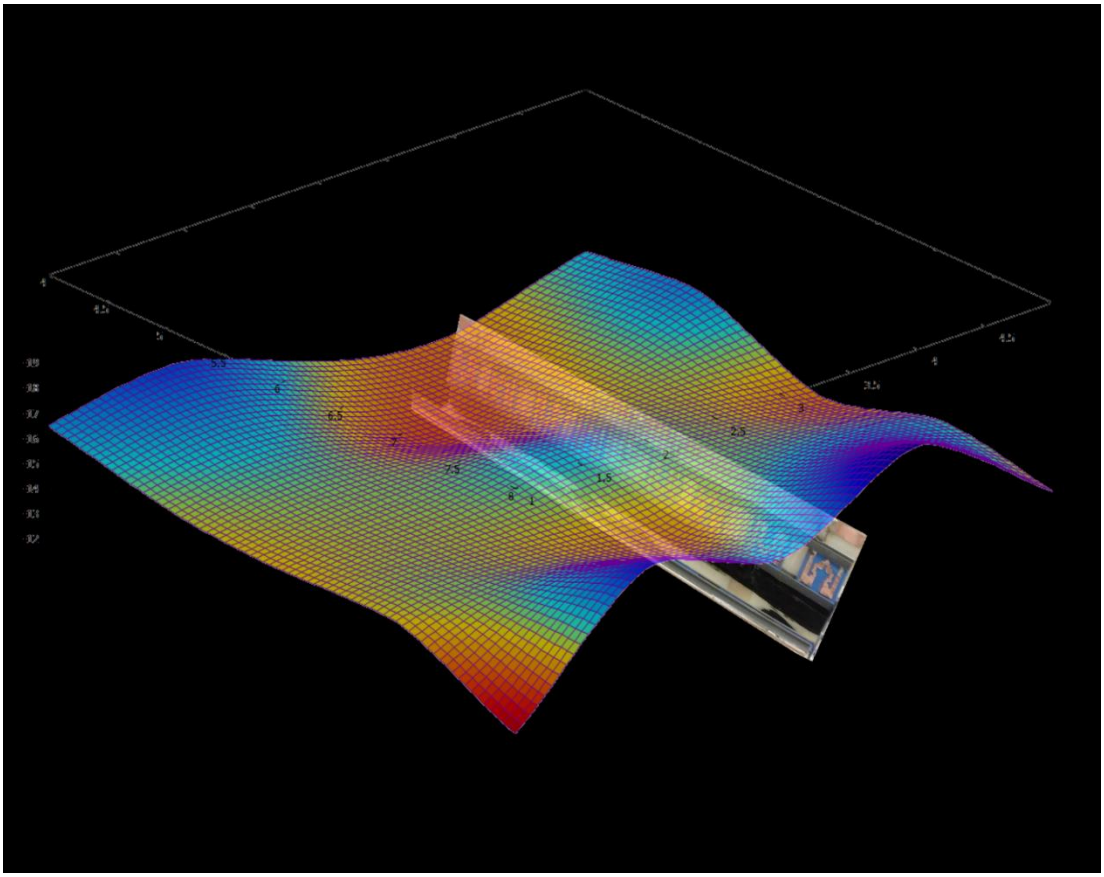

Figure 4.1.1. The derived equation $R^{00} = \frac{4\pi G}{\mu_0 c^4} \cdot B^2$ was used along with the empirical magnetic flux data collected 4 inches from the engine. The resultant area collected was 2 ½ ft. by 1 ft., 55 points of gridded data were collected over 20 seconds at 10 watts of power from the engine. The magnetic flux data is in micro Tesla's. R^{00} is the major

component of special curvature ($1/m^2$).

Examining both the Magnetic Flux and Gravity 3D images you can see the local compression effect as it bends into the VEM Drive. Within the framework of general relativity, it is possible to modify local spacetime. With the contraction of local space in front of the Drive you can see the expansion of the field beginning to curve behind. The local spacetime distortion was detected at all seven levels of data that were collected. The 4-inch level was chosen to show simply the resultant distortion. Both sets of data also show the maximum field effect that occurs over each set of the tri-pole fractal arrays.

4.2. Gravity Data

The gravity field generated by the engine was evaluated and mapped into a 3D wire mesh image. The resultant gravity field data was collected 4 inches from the bottom of the engine

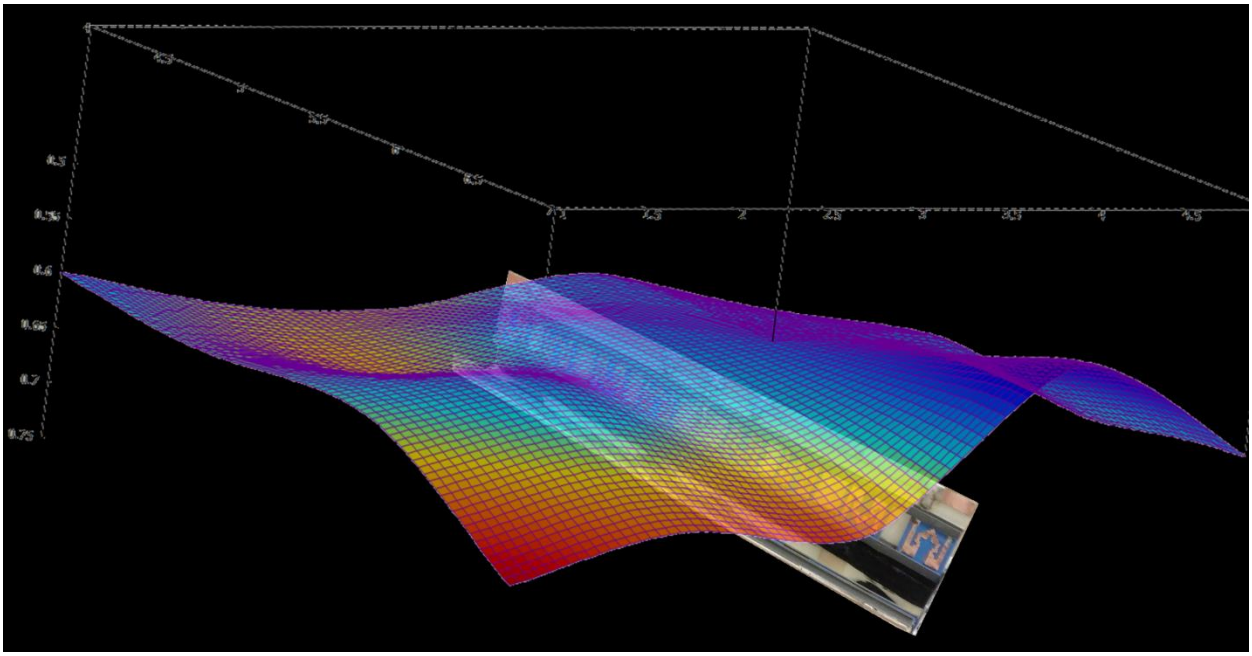

Figure 4.2.1. The 4-in. layer of raw Gravity Data shows the compression of the fabric of space into the Engine. The gravity data is measured in fractional differences of 9.8 m/s^2.

4.3. Additional Characteristics

When powering up an early Model 7 etched circuit board Drive a negative field is created for several seconds and then followed by a full-scale deflection on a Trifield™ meter. When power is released the meter deflects slightly and then indicates full positive deflection for 1.5 to 2 seconds before returning to zero. Trifield™ meter data was collected and plotted. (See Figure below). It is apparent that after power is cut, additional energy has been released from the system. This could be caused by electron puddling on the fractal arrays or we are seeing the spacetime distortion field rebounding back to a normal local space state. This phenomenon is important but requires further study.

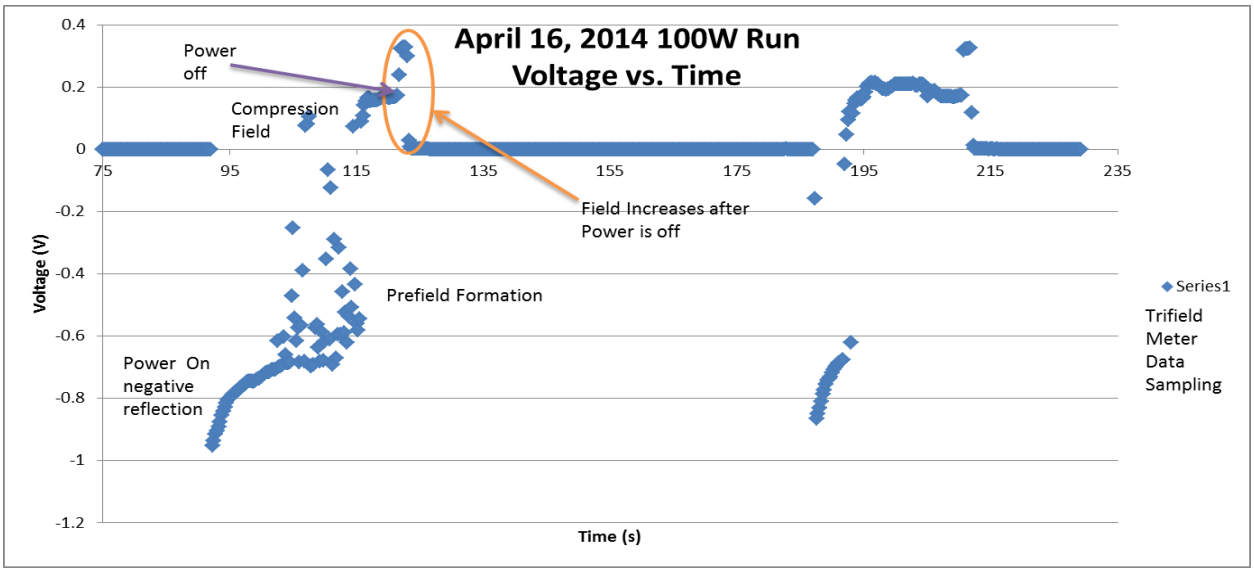

Figure 4.3.1 The time is in quarter seconds on the bottom of the chart

5. Model 15C Engine Performance

There have been 15 series of engines developed and tested. Each new series of motor has incorporated improvements and discoveries along the way. The ultimate achievement is to get a craft off the ground under its own autonomous power. The number of motors developed is reflected of that goal. The closer the R^2 value is to 1, the higher the correlation of the data. The data plot reflects a high correlation of the R^2 value of 0.9569. This signifies consistency of the data collected and that the resulting exponential curve can predict future outcomes for that motor configuration.

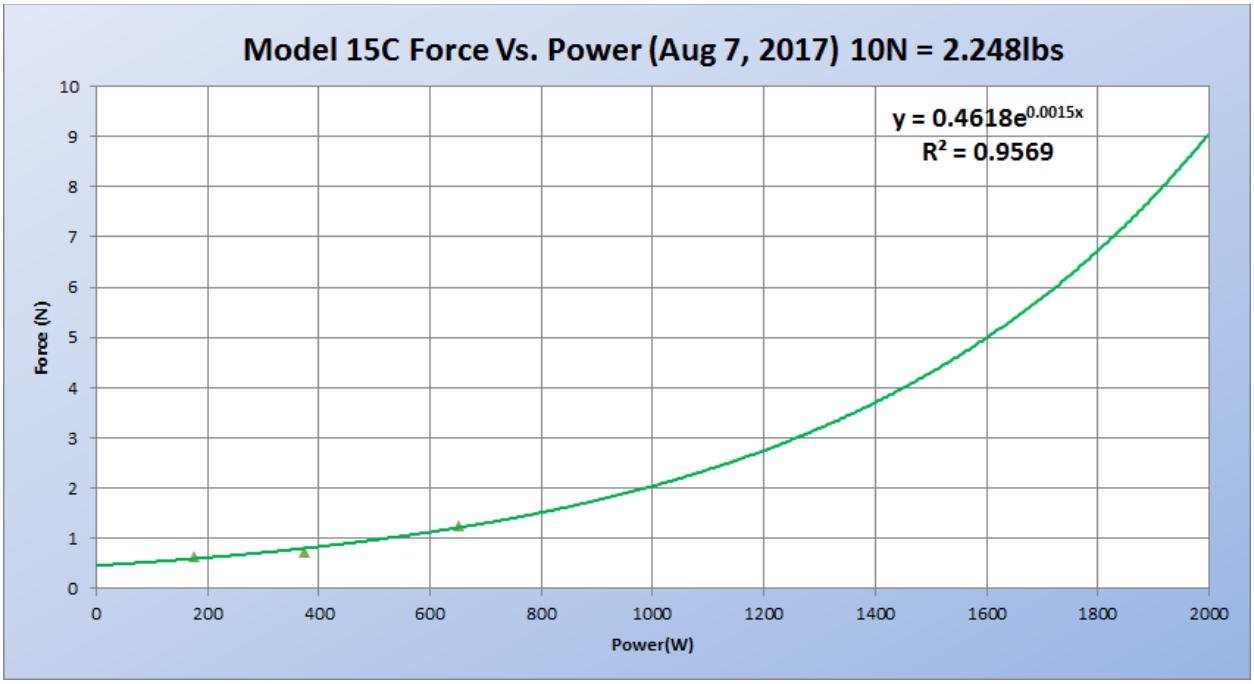

Figure 5.1. Below are the Videos that reference the graph and collect data points above conducted on August 7, 2017 for 175, 375 and 650 watts. The tests were conducted using the Model 15C VEM Drive.

The following videos are calibrated with 100g/200g(1N/2N) weight corresponding to 4.75mm/9.5mm displacement:

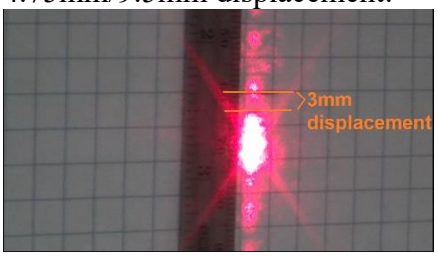

VEM DRIVE 175watt TEST
https://www.youtube.com/watch?v=Pho-aCZPAJM

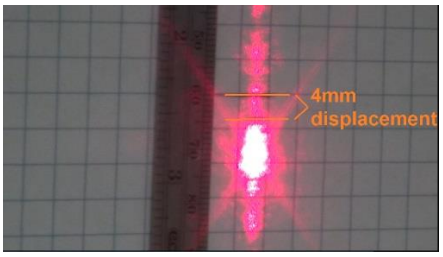

VEM DRIVE 375watt TEST
https://www.youtube.com/watch?v=Q17POieg-wc

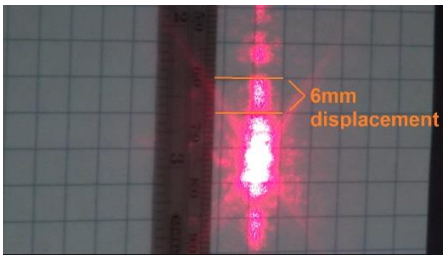

VEM DRIVE 650watt TEST
https://www.youtube.com/watch?v=h3NCNNRoqVE

The next graph identifies some recent modifications made to the Model 15C VEM Drive, which entailed changing the drives power connector to a heavier duty style. It made a difference, particularly when working in a VHF environment. Note the R^2 value is 0.9992. Continued testing and analyzing can reveal subtle improvements and advancements can sometimes be made quickly.

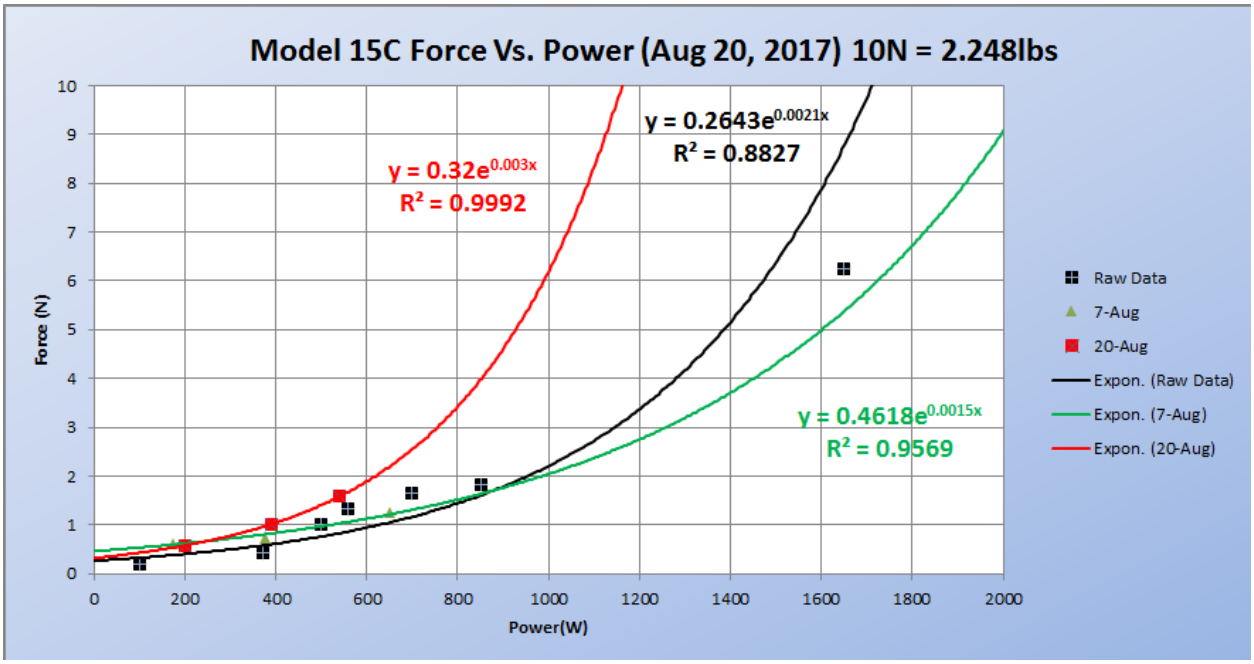

6. The VEM Drive System

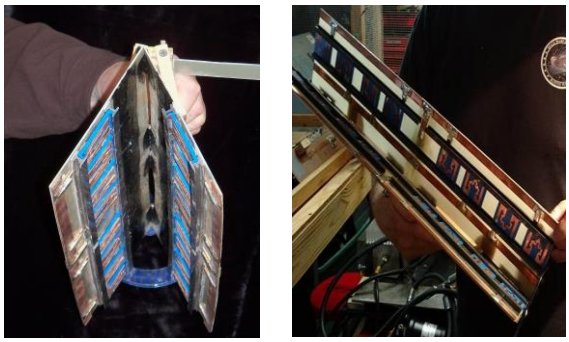

Figure 6.1. Model 15 VEM Drive

The engine is 2 ft. long x .5 ft. high with an adjustable opening at the bottom. The fractal pads that configure the four tri-pole fields can slide to configure different field affects. We have experimented with over twenty-five configurations of pad and angle openings for the Drive. There are power grids that run the total distance of the motor. These grids provide the feeds for the various Tri-pole field configurations. Semi rigid cable is used to send RF energy to the motor. The motor is suspended in a Faraday Cage by a central spring and additional spring for the RF cable feed. A deep Earth bentonite based ground rod system was used to contain any spurious signals from the motor. All equipment for the Drive is also grounded to this system. For the following data graphs and charts described below, the angle was set to 60 degrees which was a 5-inch opening at the bottom of the engine. It should be noted that the engine is a pulling engine. It does not thrust, is battery powered and uses zero propellant. The VEM Drive is silent.

6.1. VEM Drive System Layout

Throttle **Linear Amps** **Battery Pack**

The VEM Drive has an electronic throttle control. The throttle can operate manually or under software control. The system has low and high-power control settings. The design has many features to accommodate many system and power configurations. Automatic limits can be set to turn off the motor if met. The exciter and the throttle, control the RF linear amplifiers power output. Single, dual and quad RF linear' s can be used to configure the Drive up to 4000 watts of power. The system runs on a 48 Volts 160 Amp Hour battery capacity. All the RF linear amplifiers can be powered with the battery system. The system can run on wall power as well, however since operating in outer space is our goal, it was decided to design and configure the whole system for battery power. Although the system can be configured to handle up four linear amps, using two multi-port RF power combiners. We use single and dual configurations for testing new upgrades to the system. The object is to reduce input power and increase

compression of the fabric of space. Once all design goals are satisfied we will move into a higher order of power. The multiple tests that have been performed to date shows an exponential relationship to power and work, which means more lifting capability. The power input to the VEM Drive that has been tested ranges from 0 to 1800 watts of power. Once over unity is achieved on a macro scale, more compression can be done with just a slight increase in power. That relationship alone will change the way we look at propulsion and its subsequent evolving technology.

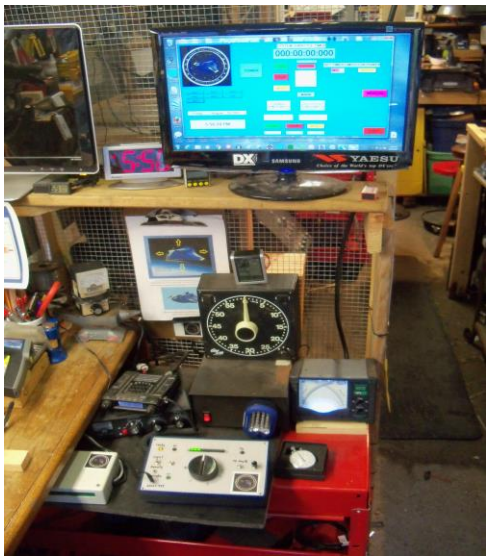

Figure 6.1.1. Flight Control System Configuration

From the exciter and throttle, the output signal goes to the four-way splitter for input to each of the RF Linear Amps that are on-line.

The RF Amps have been custom designed to work in this unique environment. The output from the Amp(s) go to the tuner section. The tuner section is tuned specifically for the variable configuration of the VEM Drive.

System Tuner

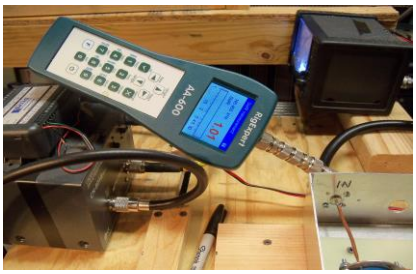
AA-600 Analyzer, SWR 1:1.01


Adjustable Fractal Pads


Power Meter

A Standing Wave Ratio (SWR) of 1:1 or 1:1.01 at 50 Ohms is the desired goal. The Drive can open at a variety of angles and the fractal tri-pole elements can also be varied in their spacing. When potential settings are made it requires the system to be re-tuned. The system can run under automated or manual control. A series of 30 to 3000 watt, dual forward and reflected power meters are used to monitor system power.

6.2. Thermal Heat Signatures

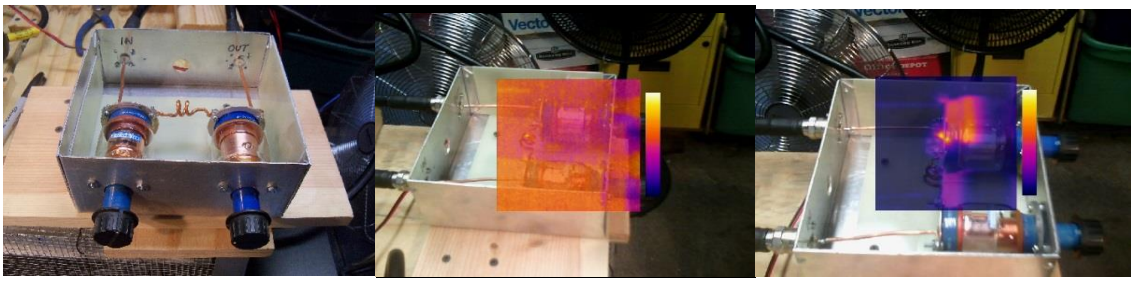
Figure 6.2.1 375-watt test run, before and after thermals images of tuner (with SWR 1:1.01)


Figure 6.2.2. 375-watt test run, before and after thermals image of VEM Drive

The output side of the tuner can handle up to 15KV and 45 Amps of power. The after thermal of the tuner shows it can get warm in spots. However it will hold tune above 2300 watts of power. The VEM Drive after thermal shows a heating of two retainer screws which is not part of the motor it holds the angle retainer in place on a standoff wood block. The internal open v cavity has the same temperature as the ambient air. The motor does not make any sound.

6.3. Radiation Measurements

Measurements have been made during testing and just a minimal amount of micro Rads of emitted radiation have been detected. A digital Giger counter and a Victor 712 with muller tube have been used to monitor any output. After tests at high and low power without any significant results, we have discontinued using the meters on normal testing runs.

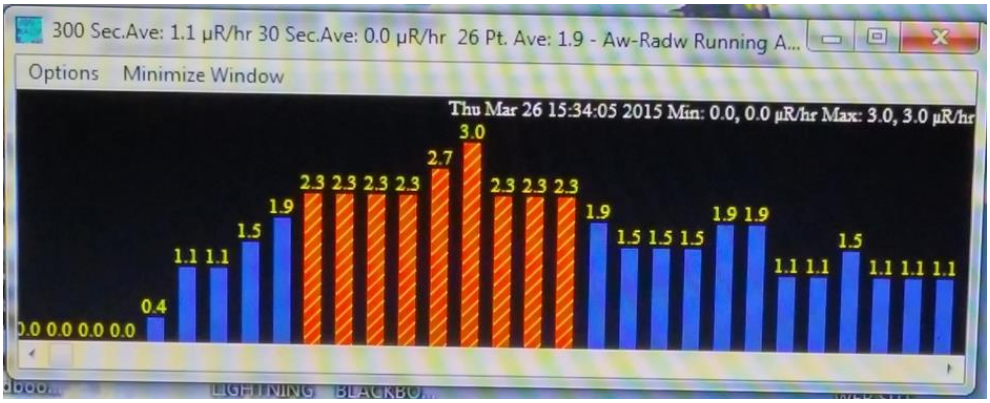

Figure 6.3.1.
Rad (radiation absorbed dose)1 rad = 100 erg/gram
Radiation of 1.1 micro Rad were measured at 100 watts.
Environmental background radiation is 12 to 18 micro Rad.

7. Fractal Arrays

Fractal arrays provided a very minimal flexible footprint that still allowed for substantial power levels that would be used in testing. The individual fractal elements are based on a modified 4th iteration of a fractal Koch curve. The fractal elements were designed to match the frequencies collect from empirical thunderstorm investigations (Pares 2008 – 2010). The 146 MHz VHF frequency range was used as a base design for the fractal arrays. The angle of the VEM Drive is dependent on fractal pad/tri-pole field spacing and the amount of power being applied.

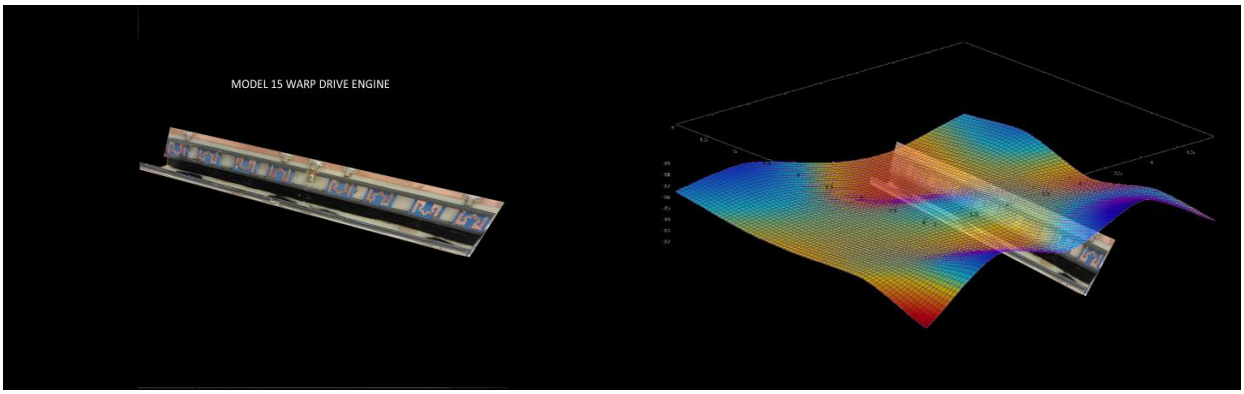

Figure 7.1 Model 15 Fractal Array Layout and corresponding magnetic flux compression field.

Several fractal iterations were tested successfully. The 4th fractal iteration had the best response and most robust properties.

Figure 7.2. Dual fractal pattern of tri-pole arrays. Notice that the fractal pads slide on a channel, which uses a via and slide bar under the pad to adjust the fractal tri-pole arrays.

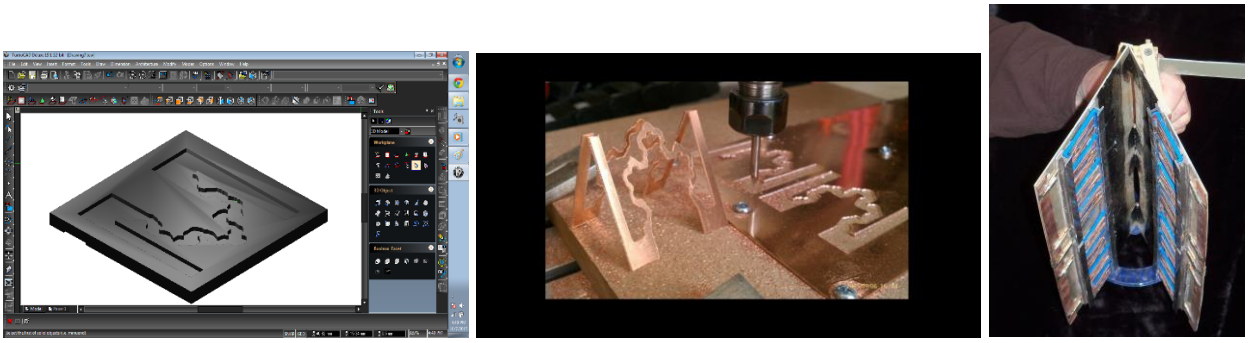

8. Error Accountability

Air Currents

Our laboratory facility has an open-air environment. The VEM Drive is suspended by central spring and surrounded by a wire mesh faraday cage. Air currents are negligible when testing, however we avoid testing outside of the realm of a ±.03mm displacement on our projection screen. This would account for less than a ±.01N difference in our Force vs Power tests. When preforming our Cavendish Experiments air currents are negated completely since the moving torsion bar is suspended and is enclosed inside our electrically insulated box.

External RF Interactions

Since the entire device is surrounded with a very well-grounded faraday cage there is not any influence from external sources. The surrounding area in the Lab is monitored by Tri-Field and frequency meters. No source of external RF transmissions have been detected in the area.

Thermal expansions

Thermal expansion and compression happens to any object that changes temperature. In our experiments, there are few parts that can expand to change our results. Before and after a run we use a IR Thermal imager to scan the entire system which reports less than a 1-degree Celsius change in temperature throughout the system. For the parts that can expand, there is less than ±.000034mm displacement. This could produce a difference of ±.0000113N in the results.

Vibration

Vibrations can alter the recorded measurements when observed in the system. Vibrations are not likely but if they occur, they could account for a displacement of ±.025mm. This would result in a difference of ±.0083N.

Human Error

Human error can account for some differences in recording measurements. Between multiple runs and self-error checking, the comparative displacement error caused from measuring would be ±.05mm. This would produce results at ±.016N.

9. Analysis

The VEM Drive creates a pulling action within the framework of general relativity. The data collected shows an artificial inducement to compress local space in front of the drive and expand behind. This tendency lends to the existence of creating a local space warp bubble. Preliminary findings confirm the hypothesis that the resultant VEM Drive produces a pulling force. As the research proceeded it was found that a laser beam could be compressed when passed through the VEM Drive and via an interferometer. Further investigation indicated a Redshift of the frequency and wave length into the open cavity of the VEM Drive. This was a major early discovery that indicated that the local fabric of space was compressed. Additional verification was also confirmed when the VEM Drive local compression field displaced non-metallic and metallic objects on a torsion bar through the walls of a glass and wood containment case. The effects were still measurable at 140 cm from the Drive just using 25 watts of power. The pulling nature of the Drive is established. A compression of the fabric of space appears to be present in a micro environment even using low power. As new drives were developed and data collected it was shown that the Power to work ratio is exponential. It was noted that more output compression can be done with just a slight increase in power. Variation in pad spacing and drive opening can also change power to work output. Tests were also performed to evaluate axial control for maneuvering a potential spacecraft. This can be achieved by adjusting the strength of the fields for each motor (up down, sided to side and reverse). These tests also indicated that larger local warp bubbles can be created by using multiple motor sources. During these tests, a digital Giger counter and a Victor 712 with muller tube were used to monitor any output radiation. A small amount of radiation has been detected. Radiation of 1.1 micro Rad were measured at 100 watts. Environmental background radiation is 12 to 18 micro Rad.

Rad (radiation absorbed dose) 1 rad = 100 erg/gram

The near field reactants of the VEM Drive is a powerful artificial inducement which can create a compression field of spacetime. The fractal tri-pole electric fields can adjust the near field reactants. This is accomplished using a throttle control and a 48 Volt, 160 Amp Hour battery pack. The pulling-to-power results, at 20 seconds of continuous power are .19 N at 100 watts to 6.25 N at 1650 watts mode at 146 MHz for VEM Drive. The list of experiments and results presented in this paper support the validity of this claim. The variable design of this drive allows for future exploration and development. A further comparison will be made between other Ion and EM Drives.

The following is a summary from a recent paper released about NASA's EM Drive

"The current state-of–the-art thrust to power for a Hall thruster is on the order of 60mN/kW60 mN/kW. This is an order of magnitude higher than the test article evaluated during the course of this vacuum campaign; however, for missions with very large delta-v requirements, having a propellant consumption rate of zero could offset the higher power requirements. The 1.2mN/kW1.2 mN/kW performance parameter is over two orders of magnitude higher than other forms of "zero-propellant" propulsion, such as light sails, laser propulsion, and photon rockets having thrust-to-power levels in the 3.33–6.67μN/kW3.33–6.67 μN/kW (or 0.0033–0.0067mN/kW0.0033–0.0067 mN/kW) range." (White, et al 2017)

The VEM Drive pulling-to-power results, at 20 seconds of continuous power are .19 N at 100 watts to 6.25 N at 1650 watts mode at 146 MHz for the Drive. The comparison in the chart below was based on 650 watts of power for 20 seconds, which yielded 1.26 N or 1260 mN.

							SWD Calculations		
Engine	µN	mN	Seconds	Watts	mN / kW (Scaled)		mN / Watt	mN / Sec	µN / Sec / Watt
Dawn NSTAR*	91000	91	3100	2100	(2.3)		0.0433333	0.029355	0.013978495
NASA EM	12000	12	24s - over 1min	80	(1.2)	**	0.15	0.2	2.5
Hall Thuster*	600000	600	60	10000	(60)		0.06	10	1
Japan's Hayabusa 2 (Ion)*	10000	10	2800	1200	(12)		0.0083333	0.003571	0.00297619
SWD VEM Drive	1260000	1260	20	650	(1938.462)		1.9384615	63	96.92307692

*use fuel consumption
**predicted force magnitude using slope-filtering plot with aggressive slope-filter level
** 60 seconds used for NASA EM
() Reported Values

Dawn: https://dawn.jpl.nasa.gov/missihttps://www.pddnet.com/blog/2015/03/spacecraft-week-dawnon/ion_prop.asp
Nasa: https://arc.aiaa.org/doi/10.2514/1.B36120
Hall: https://www.science.gov/topicpages/x/xenon+ion+propulsion
http://www.nature.com/scientificamerican/journal/v300/n2/full/scientificamerican0209-58.html?foxtrotcallback=true
Hayabusa 2 http://spaceflight101.com/spacecraft/hayabusa-2/

Figure 9.1 When compared to both Ion and EM Drives raw values and the base scaling for 1000 watts for all devices in the chart above, the VEM Drive produces more capability with less power and zero fuel.

10. Conclusions

This paper described a new solid-state, zero propellant, radio-frequency (RF) resonant, variable near field reactants, Variable Electro Magnetic Drive (VEM) Drive. The VEM Drive can create a pulling action within the framework of general relativity. The data collected shows an artificial inducement to compress local spacetime. This tendency lends to the existence of creating a local space warp bubble and preliminary findings confirm the hypothesis that the resultant VEM Drive produces a pulling force. Examining both the Magnetic Flux and Gravity 3D images, shows the local compression effect which bends into the VEM Drive. Within the framework of general relativity, it is possible to modify local spacetime. With the contraction of local space in front of the Drive the expansion of the field begins behind. The local spacetime distortion was detected at all seven levels of data that were collected. The 4-inch level was chosen to show the resultant distortion. Both sets of data also show the maximum field effect that occurs over each set of the tri-pole fractal arrays.

The near field reactants of the VEM Drive is a powerful artificial inducement which can create a compression field of spacetime. The fractal tri-pole electric fields can adjust the near field reactants. This is accomplished using a throttle control and a 48 Volt, 160 Amp Hour battery pack. **The pulling-to-power results, at 20 seconds of continuous power are .19 N at 100 watts to 6.25 N at 1650 watts mode at 146 MHz for VEM Drive.** The list of experiments and results support the validity of this claim. The variable design of this drive allows for future exploration and development.

								SWD Calculations		
Engine	µN	mN	Seconds	Watts	mN / kW (Scaled)			mN / Watt	mN / Sec	µN / Sec / Watt
Dawn NSTAR*	91000	91	3100	2100	(2.3)			0.0433333	0.029355	0.013978495
NASA EM	12000	12	24s - over 1min	80	(1.2)	**		0.15	0.2	2.5
Hall Thuster*	600000	600	60	10000	(60)			0.06	10	1
Japan's Hayabusa 2 (Ion)*	10000	10	2800	1200	(12)			0.0083333	0.003571	0.00297619
SWD VEM Drive	1260000	1260	20	650	(1938.462)			1.9384615	63	96.92307692

*use fuel consumption
**predicted force magnitude using slope-filtering plot with aggressive slope-filter level
** 60 seconds used for NASA EM
() Reported Values

Dawn: https://dawn.jpl.nasa.gov/missihttps://www.pddnet.com/blog/2015/03/spacecraft-week-dawnon/ion_prop.asp
Nasa: https://arc.aiaa.org/doi/10.2514/1.B36120
Hall: https://www.science.gov/topicpages/x/xenon+ion+propulsion
http://www.nature.com/scientificamerican/journal/v300/n2/full/scientificamerican0209-58.html?foxtrotcallback=true
Hayabusa 2 http://spaceflight101.com/spacecraft/hayabusa-2/

Experiment Results Summary

1. Compression of a laser beam through the VEM Drive and via an interferometer.
2. Redshift of the frequency and wave length into the open cavity of the VEM Drive. The local field was compressed.
3. VEM Drive local compression field displaced non-metallic and metallic objects on a torsion bar through the walls of a glass and wood containment case. The effects were still strong at 140 cm from the Drive. The pulling nature of the Drive is established.

A compression of the fabric of space appears to be present in a micro environment even using low power.

4. Power to work is exponential. Once over unity is achieved on a macro scale, more work can be done with just a slight increase in energy.
5. Variation in pad spacing and drive opening can change power to work output.
6. Axial control for maneuvering can be achieved by adjusting the strength of the fields for each motor (up down, side to side and reverse).
7. Larger local warp bubbles can be created by using multiple motor sources.
8. Radiation of 1.1 micro Rad were measured at 100 watts. Environmental background radiation is 12 to 18 micro Rad.
   Rad (radiation absorbed dose) 1 rad = 100 erg/gram

11. Links for Space Warp Dynamics Video's

1) VEM DRIVE 175w TEST
https://www.youtube.com/watch?v=Pho-aCZPAJM

2) VEM DRIVE 375w TEST
https://www.youtube.com/watch?v=Q17POieg-wc

3) VEM DRIVE 650w TEST
https://www.youtube.com/watch?v=h3NCNNRoqVE

4) 4 Minute Video

OVERVIEW OF THE POSTED PAPER
WITH RECORDED VIDEOS OF Model 15C VEM DRIVE TESTS August 7, 2017

https://www.youtube.com/watch?v=KNcKgRQv09A

5) 2015 Cavendish Experiment Video

https://www.youtube.com/watch?v=6X8Q4QW7ggA

12. Epilogue

The small steps reported in this series of investigations and laboratory experiments provide the first stepping stone in the evolution of space warp technologies. The progress made to date is expensive and time consuming. The introduction of Model 16 is near completion which will allow higher power testing than ever before. We plan to power this motor with up to 4000 watts of power. Our goal of lifting a small craft off the ground is still within our limited resources. Larger and more powerful VEM Drive engines are being designed and developed for the completion of the autonomous Bluebird II UAV. The full-size Bluebird II will be a seven-passenger craft. As warp technology evolves, the goal is to go faster than light utilizing a space warp environment. At that point imagine the possibilities. Will space, then, be the final frontier?

Fluctui Futuro
The wave of the future

Bluebird II UAV

13. References

Alcubierre, M. (1994). The warp drive: hyper-fast travel within general relativity. *Classical and Quantum Gravity*, 11(5), L73-L77.

Hiscock, W. A. (1997). Quantum effects in the Alcubierre warp-drive spacetime. *Classical and Quantum Gravity*, 14(11), L183-L188.

MacGregor, R., & Gernon, B. (2005). The fog: A never before published theory of the Bermuda Triangle phenomenon. Woodbury, Minn.: Llewellyn Publications.

MacGregor, R., & Gernon, B. (2017). Beyond the Bermuda Triangle. Wayne, NJ.: The Career Press, Inc.

Musha,T. M. Y. (2011). Field Propulsion System for Space Travel. SAIF Zone: Bentham Science Publishers. Retrieved July 10, 2017, from http://ebookcentral.proquest.com/lib/unomaha/detail.action?docID=864250 , Page 126 *Physics of Non-Conventional Propulsion Methods for Interstellar Travel Musha and Minami* APPENDIX.D

NASA/Jet Propulsion Laboratory. (2013, November 8). It's complicated: Dawn spacecraft spurs rewrite of asteroid Vesta's story. *ScienceDaily*. Retrieved June 27, 2014, from http://www.sciencedaily.com/releases/2013/11/131108091328.htm

Natário, J. (2002). Warp drive with zero expansion. *Classical and Quantum Gravity*, 19(6), 1157-1165.

Obousy, R. K. & Cleaver, G. (2007). Warp drive: a new approach. Baylor University, Waco, Texas, 76706, USA

Pares, D. (2010). Bruce Gernon. Robert Mcgregor. Retrieved July 20, 2017, from http://www.spacewarpdynamicsllc.com/blank-zb9d2

Pfenning, M. J., & Ford, L. H. (1997). The unphysical nature of `warp drive'. Classical and Quantum Gravity, 14(7), 1743-1751.

Puthoff, H. E. (1996). SETI, the Velocity ‐ of ‐ Light Limitation, and the Alcubierre Warp Drive: An Integrating Overview. *Physics Essays*, 9(1), 156-158.

Taylor, T. S. & Powell, T. C. (2003). Current status of metric engineering with implications for the warp drive. 39th AIAA/ASME/SAE/ASEE Joint Propulsion Conference and Exhibit. Huntsville, Alabama.

University of Adelaide. (2012, October 10). Extending Einstein's theory beyond light speed. *ScienceDaily*. Retrieved June 27, 2014, from http://www.sciencedaily.com/releases/2012/10/121010092742.htm

Van den Broeck, C. V. (1999). A `warp drive' with more reasonable total energy requirements. *Classical and Quantum Gravity*, 16(12), 3973-3979.

Warp Drive - could such a thing actually be built?. (n.d.). Guide to the Universe. Retrieved July 21, 2014, from http://www.guide-to-the-universe.com/warp-drive.html

White, H. at. el. (2017). Measurement of Impulsive Thrust from a Closed Radio-Frequency Cavity in Vacuum Harold. *Journal of Propulsion and Power*. Retrieved July 21, 2017, from https://arc.aiaa.org/doi/10.2514/1.B36120

14. Appendix A

The Research and Development team has been together for over four years. The success of the research has motivated the team to apply for and receive a patent pending from the US Patent Office. Within the last four years, the team has formed a company called Space Warp Dynamics, LLC. Reference Space Warp Dynamics, LLC website at http://www.spacewarpdynamicsllc.com/ for additional information.

Background for David Pares, Matt Judah, Kyle Finley

David: Air Force Meteorology, Defense Contracting, Lone Eagle Systems Incorporated, University Adjunct at four Colleges (Meteorology, Astronomy, Geography, Geology and Physics,). Self-funded research linear displacement space warp, US Patent Pending (Space Warp Motor, Pares/Judah, Official patent pending notice number 61/960001), Space Warp Dynamics, LLC formation (President). Additional background in: Electronics, Software, Hardware, Ham Radio and Aviation (Commercial Pilot/Instructor).

Education: AS Engineering Science OCCC Middletown NY, BGS Geography University of Nebraska at Omaha, MS Geography University of Nebraska.

Matt: Space Warp Researcher, BS Physics University of Nebraska at Omaha, MS Physics Colorado State at Fort Collins CO. PhD Physics program Colorado State at Fort Collins CO. US Patent Pending (Space Warp Motor Pares/Judah), Space Warp Dynamics formation (Vice President)

Kyle: Space Warp Researcher, BGS Computer Engineering, University of Nebraska at Omaha. Additional background in: Information Assurance, Graphic Design, System Design Software, Analog and Digital Engineering.

Photo Credit

Thanks to Laura Wegrzyn for diagrams 4.0 and 4.2 as well as work on the logo design.